

## Hard and precision QCD measurements at HERA

Günter Grindhammer for the H1 and ZEUS Collaborations

Max-Planck-Institut für Physik, Föhringer Ring 6, 80805 München, Germany

### Abstract

Recent results on the combination of open charm and beauty production data in deep-inelastic scattering and their comparison to perturbative QCD calculations at next-to-leading order and approximate next-to-next-to-leading order are presented. The combined data are used to extract the masses of the charm and beauty quarks at next-to-leading order. Inclusive jet and dijet cross sections in deep-inelastic scattering are used to extract the strong coupling  $\alpha_s(m_Z)$  at next-to-next-to-leading order for the first time. Finally, further new observables measured for the description of prompt photons plus jet production in deep-inelastic scattering and their comparison to perturbative QCD calculations are shown.

**Keywords:** deep-inelastic scattering, charm production, beauty production, jet production, quantum chromodynamics, next-to-next to leading order, strong coupling constant

**PACS:** 13.60.Hb, 13.60.-r, 13.87.Ce, 12.38.Qk, 14.65.Dw, 14.65.Fy

### 1. Introduction

HERA was the only  $ep$ -collider and together with the H1 and ZEUS experiments allowed to investigate a wide range of physics and processes in deep-inelastic scattering (DIS), diffractive scattering (DIFF) and photoproduction (PHP) with significant precision, and thus provided for example a deeper understanding of quantum chromodynamics (QCD). The energy of the  $e^-$  or  $e^+$  beam was 27.6 GeV, and the energy of the proton beam, for the data being discussed here, was first 820 and later 920 GeV with a center-of-mass energy of 318 GeV. The H1 and ZEUS experiments collected a combined data sample of  $\sim 1 \text{ fb}^{-1}$  in the years from 1992-2000 (HERA-I) and 2003-2007 (HERA-II). Both experiments provide well calibrated datasets, e.g. the hadronic energy scale uncertainty is typically  $\sim 1\%$ .

In this presentation we are concerned with hard processes in neutral current (NC) DIS. The important processes at different orders in  $\alpha_s$  in DIS are indicated in

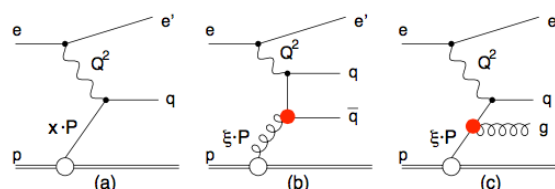


Figure 1: Basic DIS processes: a)  $O(\alpha_s^0)$ , b)  $O(\alpha_s)$  boson-gluon fusion (BGF), c)  $O(\alpha_s)$  QCD Compton (QCDC).

Fig. 1. Inclusive cross section predictions are sensitive in leading order (Fig. 1a) to the valence and sea quarks of the proton. They become sensitive to the gluon density and the strong coupling, which are however strongly correlated, only at order  $\alpha_s$  and beyond (scaling violations). Charm and beauty production at HERA are already at leading order (LO) sensitive to  $\alpha_s \otimes g$  via the BGF process (Fig. 1b), but the calculations depend even more on the value of the heavy quark masses and the heavy quark scheme used. The combination of charm and beauty cross sections from the H1 and ZEUS collaborations and the determination of the quark masses are discussed in sect. 2.

Email address: guenterg@desy.de (Günter Grindhammer for the H1 and ZEUS Collaborations)

Jets in DIS, when measured in the Breit frame [1], are also sensitive to  $\alpha_s \otimes g$  already at LO, via the boson-gluon-fusion (BGF) process. This process dominates for the negative photon momentum transfer squared or photon virtuality,  $Q^2$ , less than about 1000 GeV<sup>2</sup>. Above this value the QCDC process (Fig. 1c) becomes dominant, providing sensitivity to the strong coupling without involving the gluon from the proton. Thus, the addition of jet measurements together with hitherto determined parton distribution functions from inclusive NC and charged current (CC) measurements, allows an extraction of the strong coupling. The first precision extraction of  $\alpha_s(m_Z)$  at next-to-next-to-leading order (NNLO), using all appropriate sets of inclusive jet and dijet data sets from H1, is presented in sect. 3.

Measurements of DIS events with a prompt photon and a jet provide another, theoretically clean test of perturbative QCD, since the photon does not hadronise in contrast to the quark or gluon, and there are fewer diagrams compared to those in parton-parton processes. New results on this topic from ZEUS are presented in sect. 4.

## 2. Charm and beauty quarks

Heavy quarks and anti-quarks are produced in pairs, predominantly in BGF as illustrated in Fig. 1b). H1 and ZEUS measurements, using a variety of techniques to tag charm and beauty quarks such as: reconstructed  $D^{*+}$ ,  $D^+$  and  $D^0$  meson decays, reconstructed muons and electrons from heavy-flavour semi-leptonic meson decays, and analysis of charged tracks exploiting lifetime information, are combined to provide a single consistent HERA data set of reduced charm and beauty cross sections, in the kinematic range of photon virtuality  $2.5 \leq Q^2 \leq 2000$  GeV<sup>2</sup> and Bjorken scaling variable  $3 \cdot 10^{-5} \leq x_{Bj} \leq 5 \cdot 10^{-2}$ . The reduced cross section is defined as

$$\sigma_{\text{red}}^{Q\bar{Q}} = \frac{d^2\sigma^{Q\bar{Q}}}{dx_{Bj}dQ^2} \cdot \frac{xQ^4}{2\pi\alpha^2(1+(1-y)^2)},$$

where  $y$  is the inelasticity of the interaction.

Further details of this preliminary extended combination as well as on previous combinations and the procedures can be found in [2] and in references therein. In total 13 data sets are used of which 3 on charm are new and the 5 sets on beauty are used for the first time.

The combined data are compared to theoretical predictions obtained in the fixed-flavour-number scheme (FFNS) at next-to-leading order (NLO) using HERAPDF2.0 [3] and ABM11 [4] parton distribution

functions (PDFs) and at approximate NNLO using ABMP16 [5] PDFs.

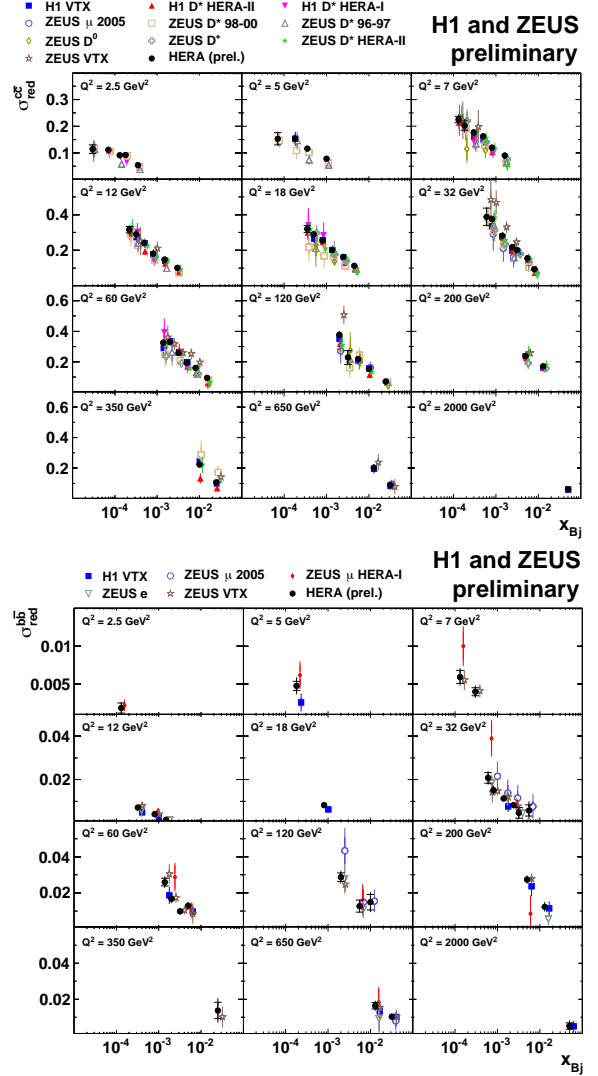


Figure 2: Combined measurements of the reduced production cross sections (full circles) for charm (upper panel) and beauty (lower panel). The inner error bars indicate the uncorrelated part of the uncertainties and the outer error bars represent the total uncertainties. The input measurements are also shown by the different markers.

In Fig. 2 the reduced charm and beauty cross section measurements, which are input to the combination, as well as the resulting combined reduced cross sections (full circles) for charm (upper panel) and beauty (lower panel) are shown as a function of  $x_{Bj}$  for different values of  $Q^2$ . The beauty data points are the first combination provided by HERA. The inputs are 209 charm and 52 beauty data points, which are combined simultaneously to yield 52 charm and 27 beauty data points. As can be

observed, the consistent treatment of correlations of statistical and systematic uncertainties, including the correlations between the charm and beauty data sets where relevant, yields a significant reduction of the overall uncertainties of the combined data.

The combined reduced cross sections  $\sigma_{\text{red}}^{Q\bar{Q}}$  (full circles) as a function of  $x_{\text{Bj}}$  for given values of  $Q^2$  are compared in Fig. 3 to NLO and approximate NNLO QCD predictions obtained using different PDFs. The data and the theory predictions are normalised to predictions using the HERAPDF2.0 set in the three-flavour-number scheme FF3A. One observes that QCD provides a reasonable overall description of the data. The dominant theory uncertainty arises from variation of the scale  $\mu_{\text{R}} = \mu_{\text{F}} = \sqrt{Q^2 + 4m_Q^2}$  by a factor of 0.5 to 2. At  $Q^2 \approx 12 \text{ GeV}^2$  the charm data points have a different slope in  $x_{\text{Bj}}$  from that of the prediction. The description of the data is not improved by the approximate NNLO prediction.

The combined charm and beauty data are used to obtain a preliminary result for the running charm and beauty masses. To this end a QCD fit is performed using a fixed three-flavour-number calculation at NLO. In addition, the NC and CC inclusive HERA DIS data are used. The light flavour PDFs are parameterised as in the HERAPDF2.0 fit. The charm and beauty masses are free parameters in the fit. The following result for the values of the masses in the  $\overline{\text{MS}}$  scheme and the fit and systematic uncertainties are obtained:

$$m_c(m_c) = 1290_{-41}^{+46} (\text{fit}) \quad {}_{-14}^{+62} (\text{mod}) \quad {}_{-31}^{+7} (\text{par}) \text{ MeV}$$

$$m_b(m_b) = 4049_{-109}^{+104} (\text{fit}) \quad {}_{-32}^{+90} (\text{mod}) \quad {}_{-31}^{+1} (\text{par}) \text{ MeV}$$

The dominant systematic uncertainty is the model one, which is dominated by the scale uncertainty as estimated by variation of the scale by a factor of 0.5 to 2. The parameterisation uncertainty is dominated by the difference between parameterising the PDFs with 13 or 14 parameters. The masses obtained are consistent with the PDG [6] masses of  $m_c = 1270 \pm 30 \text{ MeV}$  and  $m_b = 4180_{-30}^{+40} \text{ MeV}$  and consistent but significantly improved with respect to previous H1/ZEUS determinations [7, 8]. The PDG masses are mainly obtained from lattice gauge theory and time-like processes at scales in the vicinity of the heavy quark mass. An extraction of the running charm mass at different scales, using the combined charm data discussed above, is presented in [9], and the results are found to be consistent with QCD expectations.

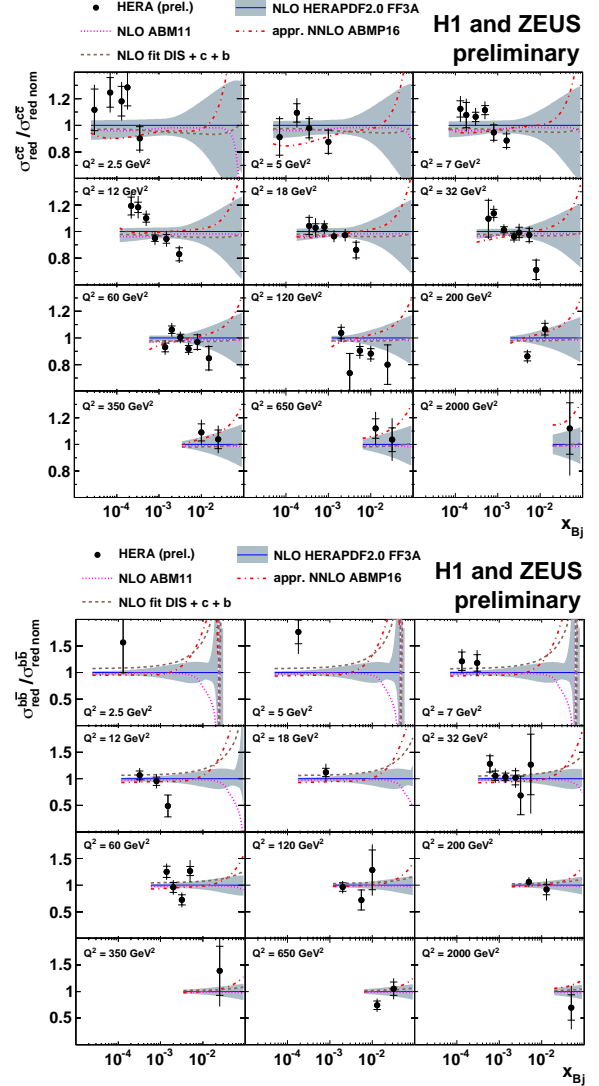


Figure 3: Combined reduced cross sections from HERA (full circles) for charm (upper panel) and beauty (lower panel) compared to NLO and approximate NNLO predictions obtained using various PDFs, normalised to predictions using the HERAPDF2.0 set FF3A.

### 3. Extraction of $\alpha_s(m_Z)$ at NNLO using jet cross sections

Since the presentation of preliminary results by H1 in my talk, the final results have become available [10]. The differences in the values for  $\alpha_s(m_Z)$  obtained are negligible, however, there are changes in the systematic uncertainties, mainly in the experimental one, due to an improved analysis strategy. Thus, the latter results are presented here.

The first program for jet production in NC DIS at NNLO, NNLOJET, has recently become available [11–13]. It is used by the H1 collaboration to extract  $\alpha_s(m_Z)$

at NNLO using its high precision measurements of inclusive jet and dijet cross sections [14–18], which cover the kinematic region  $5 < Q^2 < 15000 \text{ GeV}^2$  and  $0.2 < y < 0.7$ . Jets are defined in the Breit frame [1] using the  $k_T$  clustering algorithm [19] with a resolution parameter  $R = 1$ . The jet four-vectors are restricted to the pseudo-rapidity range  $-1 < \eta_{\text{jet}} < 2.5$  in the laboratory frame. The notations ‘300GeV’, ‘HERA-I’ and ‘HERA-II’ correspond to different data taking periods, additionally subdivided into low- $Q^2$  ( $Q^2 \lesssim 100 \text{ GeV}^2$ ) and high- $Q^2$  ( $Q^2 \gtrsim 150 \text{ GeV}^2$ ) domains, where different components of the H1 detector were used for the measurement of the scattered lepton. The inclusive jet cross sections are measured double-differentially as functions of  $Q^2$  and the jet transverse momentum  $P_T^{\text{jet}}$  in the Breit frame. For dijets at least two jets must be identified in the  $\eta_{\text{jet}}$  range above the relevant  $P_T^{\text{jet}}$  threshold. The double-differential dijet cross sections are measured as functions of  $Q^2$  and the average transverse momentum of the two leading jets,  $\langle P_T \rangle = (P_{T,1} + P_{T,2})/2$ . For more details see table 1 in [10].

The inclusive jet and dijet cross sections for a bin  $i$  in the relevant physical observables are calculated as a convolution of the PDFs  $f_k$  in the variable  $x$  and the perturbatively calculated partonic cross sections:

$$\sigma_i = \sum_k dx \int dx f_k(x, \mu_F) \hat{\sigma}_{i,k}(x, \mu_R, \mu_F) \cdot c_{\text{had},i},$$

where the sum runs over all parton flavours  $k$  and the gluon. The calculations depend on the renormalisation scale  $\mu_R$  and the factorisation scale  $\mu_F$ . The factors  $c_{\text{had},i}$  account for the hadronisation corrections. Both the  $f_k$  and the  $\hat{\sigma}_{i,k}$  are sensitive to the strong coupling. The partonic cross sections are given in terms of the perturbative expansion in orders of  $\alpha_s(\mu_R)$ . The dependence of  $f_k$  on  $\alpha_s(m_Z)$  originates from the factorisation theorem. Fixing the  $x$ -dependence of the PDFs at a starting scale  $\mu_0$  and setting  $\mu_R = \mu_F$ , the PDFs at any factorisation scale  $\mu_F$  can be calculated. The starting scale is chosen to be  $\mu_0 = 20 \text{ GeV}$ , since this is a typical scale of the jet data studied. Thus, the influence of the evolution of the PDFs on the  $\alpha_s$  determination is moderate, because  $\mu_F \approx \mu_0$ . The PDFs at that scale are well known, particularly the quark densities, because inclusive DIS at LO is independent of  $\alpha_s$ . For the PDFs at  $\mu_0 = 20 \text{ GeV}$  the NNPDF3.1 PDF set [20] is used by H1. This set was obtained with a nominal value of  $\alpha_s^{\text{PDF}}(m_Z) = 0.118$ . The scales  $\mu_R$  and  $\mu_F$  are chosen to be

$$\mu_R^2 = \mu_F^2 = Q^2 + P_T^2,$$

where  $P_T$  denotes  $P_T^{\text{jet}}$  in the case of inclusive jet cross

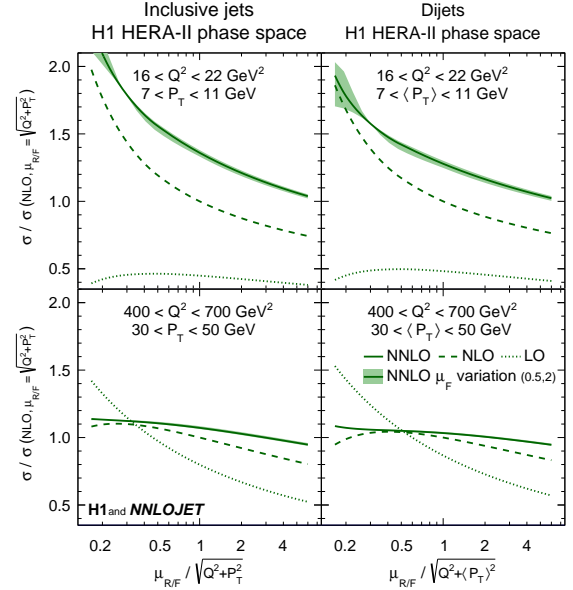


Figure 4: Relative change of jet cross section as a function of a multiplicative factor applied to the renormalisation and factorisation scale.

sections and  $\langle P_T \rangle$  for dijets. The partonic cross sections  $\hat{\sigma}_{i,k}(x, \mu_R, \mu_F)$  are calculated using NNLOJET. In Fig. 4 the scale dependence of the theory prediction at LO, NLO and NNLO, relative to that at NLO, for inclusive jets and dijets are shown for a low and a high scale region of the HERA-II data. The dependence on the scale factor is strongest for cross sections at lower values of  $\mu_R$ , i.e. lower values of  $Q^2$  and  $P_T$ . At higher values of  $\mu_R$  and at NNLO the scale dependence is almost flat.

The value of  $\alpha_s(m_Z)$  is determined in a fit of theory predictions to H1 jet cross sections [14–18] with  $\alpha_s(m_Z)$  as the single free parameter. The statistical and systematic uncertainties as well as the correlations of the uncertainties among the different data sets and running periods are taken into account. The uncertainties of the PDFs are provided by the authors of the respective parton distribution function (PDF) set.

Values of  $\alpha_s(m_Z)$  are determined separately for each individual data set, for all inclusive jet measurements, for all dijet measurements, and for all H1 jet data (referred to as H1 jets) taken together. They are shown in Fig. 5. For H1 jets the uncertainties on  $\alpha_s(m_Z)$  as a function of the parameter  $\tilde{\mu}_{\text{cut}}$ , which restricts the jet data to higher and higher scales, are shown in Fig. 6, where the minimum scale is set to  $m_b$ .

At low  $\tilde{\mu}_{\text{cut}}$  the experimental uncertainties are quite small due to the high statistics and in addition, the sensitivity to  $\alpha_s(m_Z)$  is larger due to the running of  $\alpha_s$ .

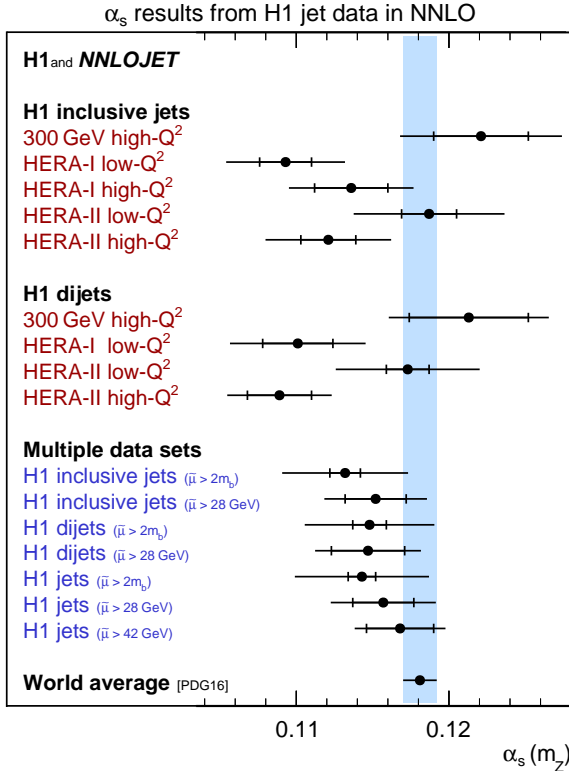


Figure 5: Summary of  $\alpha_s(m_Z)$  values obtained from fits to all H1 jet data sets. The inner error bars indicate the experimental uncertainty and the outer error bars the total uncertainty.

On the other hand, the theoretical uncertainty, estimated from the usual scale variations by a factor of 0.5 to 2.0, is large, even at NNLO. Using only data with  $\tilde{\mu}_{\text{cut}} \gtrsim 30 \text{ GeV}$ , one finds the experimental and scale uncertainty to become similar in size. Around this region of  $\tilde{\mu}_{\text{cut}}$  the PDF $\alpha_s$  uncertainty is almost negligible. H1 has chosen the value  $\tilde{\mu} > 28 \text{ GeV}$  for their main result. The H1 jets then yield the following value:

$$\alpha_s(m_Z) = 0.1157 (20)_{\text{exp}} (6)_{\text{had}} (3)_{\text{PDF}} (2)_{\text{PDF}\alpha_s} (3)_{\text{PDFset}} (27)_{\text{scale}}$$

with  $\chi^2 = 63.2$  for 91 data points. Although the reduced number of data points leads to an increased experimental uncertainty, as compared to the option  $\tilde{\mu} > 2m_b$  ( $\alpha_s(m_Z) = 0.1143 (9)_{\text{exp}} (43)_{\text{th}}$ , with the theory uncertainty being dominated by the scale uncertainty), it is still smaller than the scale uncertainty, which is found to be reduced significantly. For details on the estimation of the PDF, PDF $\alpha_s$  and PDFset uncertainties see [10]. The ratios of all H1 jet cross section measurements to NNLO predictions are displayed in Fig. 7, indicating overall good agreement between data and predictions. As shown in [10], at NNLO the distributions of the jet

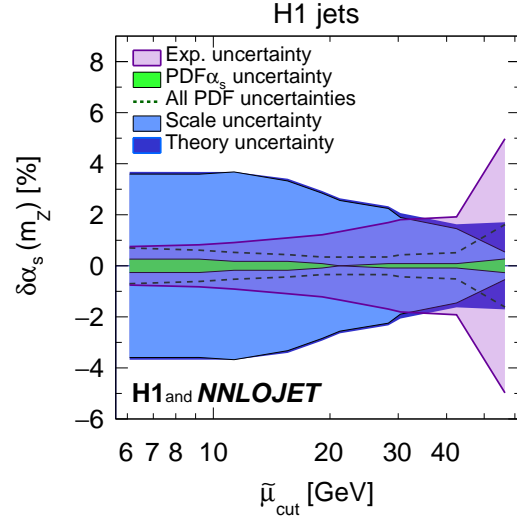


Figure 6: Uncertainties resulting from fits of  $\alpha_s(m_Z)$  as a function of the cut-off scale  $\tilde{\mu}_{\text{cut}}$  applied to the data.

$P_T$  are better described than at NLO, and the scale uncertainty is significantly reduced, particularly at higher scales.

The running of  $\alpha_s(\mu_R)$  obtained from fits to H1 jets is compared in figure 8 to other determinations of at least NNLO accuracy [21–24] and to results at NLO at very high scales [25]. The results are consistent with those of other experiments. The  $\alpha_s(m_Z)$  values found in the two approaches are consistent with each other as well as with the world average [6, 26].

The more recent H1 jet data sets [16–18] also include measurements of ratios, where the inclusive jet and dijet cross sections are normalised to the inclusive NC DIS cross section of the respective  $Q^2$  interval. In this ratio correlations of systematic and statistical uncertainties partially cancel. Therefore, normalised jet cross sections are ideally suited for studies together with inclusive NC DIS data. In addition to the approach of extracting  $\alpha_s(m_Z)$  from jets as described above, a fit of  $\alpha_s(m_Z)$  and the PDFs at NNLO is performed, using the normalised jet and the inclusive DIS cross sections from H1 as input. The fit with the requirement  $Q^2 > 10 \text{ GeV}^2$  and  $\tilde{\mu} > 2m_b$  yields the following result:

$$\alpha_s(m_Z) = 0.1142 (11)_{\text{exp,had,PDF}} (2)_{\text{mod}} (2)_{\text{par}} (26)_{\text{scale}},$$

which is largely insensitive to the PDF model and parametrisation choices. The scale uncertainty is dominating. This latter approach is also described in [10] as well as the results of the inclusion of the jet cross sections on the PDFs obtained.

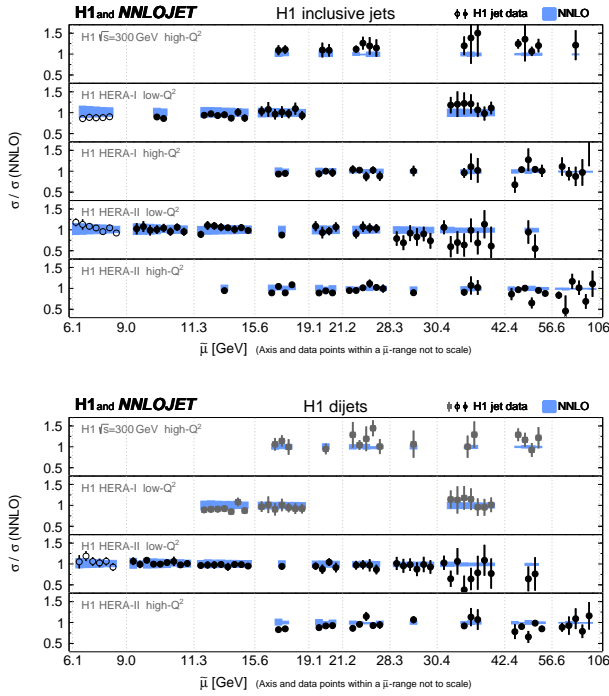


Figure 7: Ratios of H1 jet cross sections to NNLO predictions with  $\alpha_s(m_Z) = 0.1157$  as obtained from the fit to H1 jets.

#### 4. Prompt photons and jets in DIS

There are several sources of photons contributing to the hadronic final state of DIS events. Most of them arise as decay products of  $\pi^0$  or  $\eta$  mesons together with one or more jets. They may also be radiated from a quark within a jet in a fragmentation type process ( $f_{q \rightarrow \gamma}(z)$ ). These are background to the processes of interest, the production of prompt photons with high  $P_T$  as shown in Fig. 9. The photons may be radiated from the incoming or outgoing lepton (labelled LL) or be produced in hard QCD interactions (labelled QQ). The photons from LL and QQ processes are relatively isolated from other particles. The prompt QQ photons emerge directly from the hard interaction and together with jets allow a very direct test of the underlying QCD matrix elements. In order to suppress the background, isolation of the photon from the nearest charged track is required, and the widths of the photon showers in the electromagnetic calorimeter are used to discriminate against photons from meson decays. For more detailed information on the extraction of the photon signal, further details on the analysis, the variables and the new preliminary results in DIS see [27].

In this analysis a set of new variables, using combined

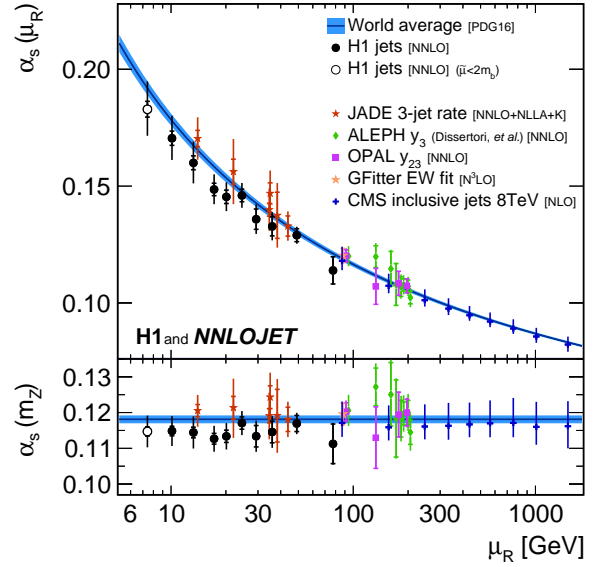


Figure 8: Running  $\alpha_s(\mu_R)$  and  $\alpha_s(m_Z)$  for fits to data points arranged in groups of similar  $\mu_R$ , compared to results from other experiments and processes and the world average (line + band).

photon-jet-electron observables, is studied. They are the following:  $x_\gamma$ , a measure of the fraction of the incoming photon energy given to the photon and jet,  $x_p$ , denoting the fraction of proton energy taken by the parton which interacts with the photon,  $\Delta\phi$ , the azimuthal angle between the prompt photon and the jet,  $\Delta\eta$ , the difference in pseudorapidity between the prompt photon and the jet,  $\Delta\phi_{e,\gamma}$ , the azimuthal angle between the prompt photon and the scattered electron, and finally  $\Delta\eta_{e,\gamma}$ , the difference in pseudorapidity between the prompt photon and the scattered electron.

The phase space of this measurement is defined by the following requirements on the virtuality of the photon  $10 < Q^2 < 350 \text{ GeV}^2$ , the transverse energy and the pseudorapidity of the photon  $4 < E_T^\gamma < 15 \text{ GeV}$  and  $-0.7 < \eta^\gamma < 0.9$ , and the transverse energy and the pseudorapidity of the jet  $E_T^{\text{jet}} > 2.5 \text{ GeV}$  and  $-1.5 < \eta^{\text{jet}} < 1.8$ .

These new results [27] allow a more detailed test of the theory compared to previous results [28]. In Fig. 10 the differential cross sections as a function of the combined photon-jet-electron variables, for the total phase space as given above, are shown and compared to Monte Carlo (MC) models, implementing leading order matrix elements and parton showers. The LL contribution is modeled using Djangoh 6 [29], with higher order QCD effects being taken into account by the colour dipole model implemented in Ariadne 4.12 [30], and

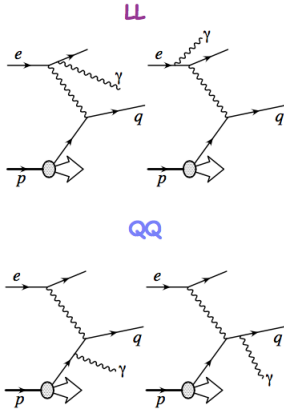


Figure 9: Lowest order prompt photon and jet production processes, with the photon radiated from the lepton (LL on top) and from the quark (QQ below).

the hadronisation of the partons is achieved by Jetset 7.4 [31], implementing the Lund string model. The QQ contribution is obtained from Pythia 6.416 [32]. These models provide a good description of the data, if the LO QQ contribution is weighted by a factor of 1.6 and the LL contribution is taken as is. The QCD prediction in the collinear factorisation approach at NLO, labelled AFG [33, 34], and the calculation implementing the  $k_T$  approach, labelled BLZ [35], are compared to the data in Fig. 11. As can be observed, the AFG prediction provides a reasonably good description of the data, while the BLZ prediction does not do so well, particularly for  $x_\gamma$  and  $\Delta\eta$ .

## 5. Conclusion

The H1 and ZEUS collaborations have provided a new combination of charm and beauty cross sections in DIS with improved precision. These HERA measurements are overall reasonably well described by NLO and approximate NNLO calculations in the fixed-flavour-number scheme. A PDF fit to the HERA charm and beauty combination as well as to the inclusive HERA cross sections yields values for the running charm and beauty masses consistent with the values from the PDG.

Sets of suitable inclusive jet and dijet measurements at low and high  $Q^2$ , obtained by the H1 collaboration during the HERA-I and HERA-II running periods, are overall well described by calculations at NLO and NNLO. At NNLO one finds an improved description of the shape of the jet  $P_T$  and a significantly reduced scale uncertainty compared to NLO, particularly

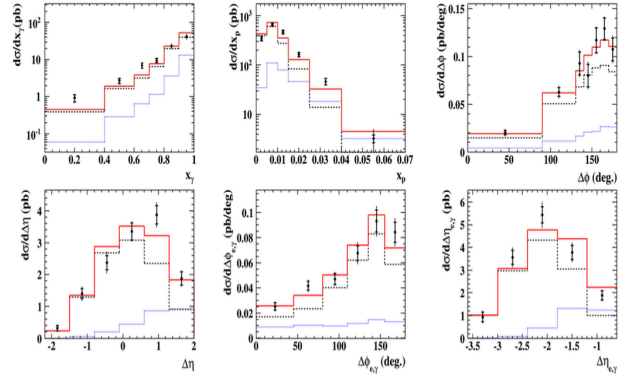


Figure 10: Differential cross section as a function of combined photon-jet-electron variables. The inner error bars indicate the statistical uncertainty, the outer error bars include also the systematic uncertainties. The solid histograms are the result of the QQ contribution from MC, scaled by a factor of 1.6 (dashed line), and the LL contribution from MC, unscaled (dotted line).

at higher scales. Using these jet data sets, restricted to high scales  $\tilde{\mu} > 26$  GeV, the strong coupling  $\alpha_s(m_Z) = 0.1157(20)_{\text{exp}}(29)_{\text{theo}}$  is extracted. This is the first precision determination of  $\alpha_s(m_Z)$  from jet data at NNLO involving one hadron in the initial state. The running of  $\alpha_s$  is tested in the range of 7 to 90 GeV, and the scale dependence is found to be consistent with the expectation.

The new observables measured for the production of prompt photons and jets in DIS are found to be well described by Monte Carlo models, employing LO matrix elements and parton showers, if the QCD contribution (QQ) is scaled up by a factor of 1.6. They are also well described by a QCD calculation at NLO, implementing standard collinear factorisation.

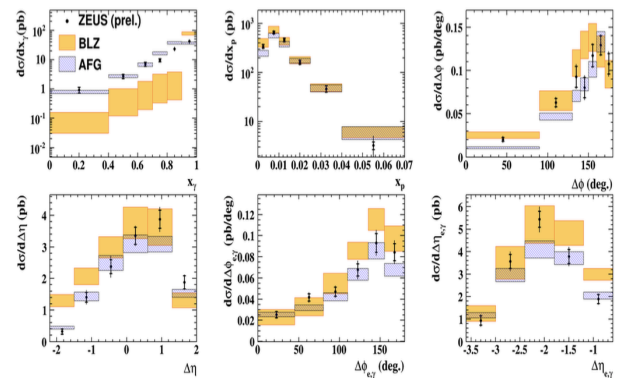


Figure 11: The data points are the same as in Fig. 10. The QCD predictions, labelled AFG (collinear factorisation) and BLZ ( $k_T$  factorisation), are shown with their respective uncertainties indicated by the shaded bands.

## References

- [1] K. Streng, T. Walsh, P. Zerwas, Quark and Gluon Jets in the Breit Frame of Lepton-Nucleon Scattering, *Z. Phys. C2* (1979) 237. doi:10.1007/BF01474667.
- [2] H1 and ZEUS collab., Combination and QCD analysis of beauty and charm production cross section measurements in deep inelastic  $ep$  scattering at HERA, H1prelim-17-071, ZEUS-prel-17-01 (2017).
- [3] H. Abramowicz, et al., H1 and ZEUS collab., Combination of measurements of inclusive deep inelastic  $e^\pm p$  scattering cross sections and QCD analysis of HERA data, *Eur. Phys. J. C75* (12) (2015) 580. arXiv:1506.06042, doi:10.1140/epjc/s10052-015-3710-4.
- [4] S. Alekhin, J. Blümlein, S. Moch, Parton Distribution Functions and Benchmark Cross Sections at NNLO, *Phys. Rev. D86* (2012) 054009. arXiv:1202.2281, doi:10.1103/PhysRevD.86.054009.
- [5] S. Alekhin, et al., Parton Distribution Functions,  $\alpha_s$ , and Heavy-Quark Masses for LHC Run II, *Phys. Rev. D96* (1) (2017) 014011. arXiv:1701.05838, doi:10.1103/PhysRevD.96.014011.
- [6] C. Patrignani, et al., Particle Data Group, Review of Particle Physics, *Chin. Phys. C40* (10) (2016) 100001. doi:10.1088/1674-1137/40/10/100001.
- [7] H. Abramowicz, et al., H1 and ZEUS collab., Combination and QCD Analysis of Charm Production Cross Section Measurements in Deep-Inelastic  $ep$  Scattering at HERA, *Eur. Phys. J. C73* (2) (2013) 2311. arXiv:1211.1182, doi:10.1140/epjc/s10052-013-2311-3.
- [8] H. Abramowicz, et al., ZEUS collab., Measurement of beauty and charm production in deep inelastic scattering at HERA and measurement of the beauty-quark mass, *JHEP* 09 (2014) 127. arXiv:1405.6915, doi:10.1007/JHEP09(2014)127.
- [9] A. Gizhko, et al., Running of the Charm-Quark Mass from HERA Deep-Inelastic Scattering Data, arXiv:1705.08863.
- [10] V. Andreev, et al., H1 collab., Determination of the strong coupling constant  $\alpha_s(m_Z)$  in next-to-next-to-leading order QCD using H1 jet cross section measurements, <http://arxiv.org/abs/1709.07251> arXiv:1709.07251.
- [11] A. Gehrmann-De Ridder, et al., The NNLO QCD corrections to Z boson production at large transverse momentum, *JHEP* 1607 (2016) 133. doi:10.1007/JHEP07(2016)133.
- [12] J. Currie, et al., NNLO QCD corrections to jet production in deep inelastic scattering, *JHEP* 1707 (2017) 018. arXiv:1703.05977, doi:10.1007/JHEP07(2017)018.
- [13] J. Currie, T. Gehrmann, J. Niehues, Precise QCD predictions for the production of dijet final states in deep inelastic scattering, *Phys. Rev. Lett.* 117 (4) (2016) 042001. arXiv:1606.03991, doi:10.1103/PhysRevLett.117.042001.
- [14] C. Adloff, et al., H1 collab., Measurement and QCD analysis of jet cross sections in deep-inelastic positron-proton collisions at  $\sqrt{s}$  of 300 GeV, *Eur. Phys. J. C19* (2001) 289. arXiv:hep-ex/0010054, doi:10.1007/s100520100621.
- [15] F. Aaron, et al., H1 collab., Jet production in  $ep$  collisions at low  $Q^2$  and determination of  $\alpha_s$ , *Eur. Phys. J. C67* (2010) 1. arXiv:0911.5678, doi:10.1140/epjc/s10052-010-1282-x.
- [16] A. Aktas, et al., H1 collab., Measurement of inclusive jet production in deep-inelastic scattering at high  $Q^2$  and determination of the strong coupling, *Phys. Lett. B653* (2007) 134. arXiv:0706.3722, doi:10.1016/j.physletb.2007.07.050.
- [17] V. Andreev, et al., H1 collab., Measurement of multijet production in  $ep$  collisions at high  $Q^2$  and determination of the strong coupling  $\alpha_s$ , *Eur. Phys. J. C75* (2) (2015) 65. arXiv:1406.4709, doi:10.1140/epjc/s10052-014-3223-6.
- [18] V. Andreev, et al., H1 collab., Measurement of jet production cross sections in deep-inelastic  $ep$  Scattering at HERA, *Eur. Phys. J. C77* (4) (2017) 215. arXiv:1611.03421, doi:10.1140/epjc/s10052-017-4717-9.
- [19] S. Ellis, D. Soper, Successive combination jet algorithm for hadron collisions, *Phys. Rev. D48* (1993) 3160. arXiv:hep-ph/9305266, doi:10.1103/PhysRevD.48.3160.
- [20] R. Ball, et al., NNPDF collab., Parton distributions from high-precision collider data, arXiv:1706.00428.
- [21] M. Baak, et al., Gfitter, The global electroweak fit at NNLO and prospects for the LHC and ILC, *Eur. Phys. J. C74* (2014) 3046. arXiv:1407.3792, doi:10.1140/epjc/s10052-014-3046-5.
- [22] G. Abbiendi, et al., OPAL collab., Determination of  $\alpha_s$  using OPAL hadronic event shapes at  $\sqrt{s} = 91 - 209$  GeV and resummed NNLO calculations, *Eur. Phys. J. C71* (2011) 1733. arXiv:1101.1470, doi:10.1140/epjc/s10052-011-1733-z.
- [23] J. Schieck, et al., JADE collab., Measurement of the strong coupling  $\alpha_s$  from the three-jet rate in  $e^+e^-$  annihilation using JADE data, *Eur. Phys. J. C73* (3) (2013) 2332. arXiv:1205.3714, doi:10.1140/epjc/s10052-013-2332-y.
- [24] G. Dissertori, et al., First determination of the strong coupling constant using NNLO predictions for hadronic event shapes in  $e^+e^-$  annihilations, *JHEP* 0802 (2008) 040. arXiv:0712.0327, doi:10.1088/1126-6708/2008/02/040.
- [25] V. Khachatryan, et al., CMS collab., Measurement and QCD analysis of double-differential inclusive jet cross sections in  $pp$  collisions at  $\sqrt{s} = 8$  TeV and cross section ratios to 2.76 and 7 TeV, *JHEP* 1703 (2017) 156. arXiv:1609.05331, doi:10.1007/JHEP03(2017)156.
- [26] S. Bethke,  $\alpha_s$  2016, in: Proceedings, 19th International Conference in Quantum Chromodynamics (QCD 16): Montpellier, France, July 4-9, 2016, Vol. 282-284, 2017, p. 149. doi:10.1016/j.nuclphysbps.2016.12.028.
- [27] ZEUS collab., Further measurements of isolated photons accompanied by jets in deep inelastic  $ep$  scattering, ZEUS-prel-16-01 (2016).
- [28] H. Abramowicz, et al., ZEUS collab., Measurement of isolated photons accompanied by jets in deep inelastic  $ep$  scattering, *Phys. Lett. B715* (2012) 88. arXiv:1206.2270, doi:10.1016/j.physletb.2012.07.031.
- [29] K. Charchula, G. Schuler, H. Spiesberger, Combined QED and QCD radiative effects in deep inelastic lepton-proton scattering: The Monte Carlo generator DJANGO6, *Comput. Phys. Commun.* 81 (1994) 381. doi:10.1016/0010-4655(94)90086-8.
- [30] L. Lönnblad, ARIADNE version 4: A Program for simulation of QCD cascades implementing the colour dipole model, *Comput. Phys. Commun.* 71 (1992) 15–31. doi:10.1016/0010-4655(92)90068-A.
- [31] T. Sjöstrand, PYTHIA 5.7 and JETSET 7.4: Physics and manual, arXiv:hep-ph/9508391.
- [32] T. Sjöstrand, S. Mrenna, P. Skands, PYTHIA 6.4 Physics and Manual, *JHEP* 05 (2006) 026. arXiv:hep-ph/0603175, doi:10.1088/1126-6708/2006/05/026.
- [33] P. Aurenche, M. Fontannaz, Photon-Jet cross sections in Deep-Inelastic Scattering, *Eur. Phys. J. C75* (2) (2015) 64. arXiv:1411.4878, doi:10.1140/epjc/s10052-015-3296-x.
- [34] P. Aurenche, M. Fontannaz, Photon-jet correlations in Deep-Inelastic scattering, *Eur. Phys. J. C77* (5) (2017) 324. arXiv:1704.08074, doi:10.1140/epjc/s10052-017-4910-x.
- [35] S. Baranov, A. Lipatov, N. Zotov, Deep inelastic prompt photon production at HERA in the kt-factorization approach, *Phys. Rev. D81* (2010) 094034. arXiv:1001.4782, doi:10.1103/PhysRevD.81.094034.